Decay rate of triaxially deformed proton emitters

Cary N. Davids and Henning Esbensen
Physics Division, Argonne National Laboratory, Argonne, Illinois 60439, USA
(Received 7 November 2003; published 10 March 2004)

The decay rate of a triaxially deformed proton emitter is calculated in a particle-rotor model, which is based on a deformed Woods-Saxon potential and includes a deformed spin-orbit interaction. The wave function of the $I=7/2^-$ ground state of the deformed proton emitter ^{141}Ho is obtained in the adiabatic limit, and a Green's function technique is used to calculate the decay rate and branching ratio to the first excited 2^+ state of the daughter nucleus. Only for values of the triaxial angle $\gamma<5°$ is good agreement obtained for both the total decay rate and the 2^+ branching ratio.

DOI: 10.1103/PhysRevC.69.034314 PACS number(s): 21.10.Tg, 23.50.+z, 27.60.+j

I. INTRODUCTION

The fundamental simplicity of the proton decay process in nuclides whose ground states are unstable to proton emission has enabled a good deal of nuclear structure information to be obtained on nuclei beyond the proton drip line [1]. The observable quantities are the proton energies and half-lives. In the rare-earth region, the proton emitters are predicted to have large static quadrupole deformations [2]. For these cases, analysis of the measurements has been carried out using a particle-rotor model, with the unbound proton interacting with an axially symmetric deformed core [3–11]. The result of such analyses over the past several years has been to obtain a good description of the ground-state properties of deformed rare-earth proton emitters, including deformations, occupation factors, Nilsson orbitals for the decaying protons, and wave function decompositions.

Adding to the information provided by the observation of decay protons, recent measurements have been made of the level structure of the deformed proton emitter ^{141}Ho by means of in-beam γ-ray spectroscopy [12]. Particle-rotor calculations of the energy levels in the rotational band lying above the $I=7/2^-$ ground state suggest that better agreement with experiment would be obtained if the nuclear shape possessed a small amount of static triaxial deformation [12]. From the standpoint of proton radioactivity it is therefore of interest to investigate the effect of a static triaxial deformation on the decay rate of a deformed proton emitter. In this work we present such an analysis, and obtain numerical results for the decay rate of the deformed proton emitter ^{141g}Ho. Preliminary results have been reported in Ref. [13]. Kruppa and Nazarewicz have also investigated the role of nonaxial effects in ^{141g}Ho decay, by introducing coupling between the ^{140}Dy ground-state rotational band and a low-lying $K=2$ γ-vibrational band [14].

II. COUPLED EQUATIONS IN THE *R* REPRESENTATION

We generalize the treatment of Esbensen and Davids [11], extending it to include the case of nuclei without axial symmetry. Using Eq. (5A-2) of Ref. [15], we write the wave function of an odd-*A* even-*N* nucleus consisting of a proton coupled to an even-even triaxially deformed rotor, in the laboratory (space-fixed) system as

$$\Psi_{IM}(\mathbf{r},\omega)=\sum_{ljR\tau}\frac{\phi^I_{ljR\tau}(r)}{r}|ljR\tau IM\rangle, \tag{1}$$

where l and j are the orbital and total angular momentum of the particle, R and τ are the rotational quantum numbers of the rotor, and I is the total angular momentum of the nucleus ($\mathbf{I}=\mathbf{j}+\mathbf{R}$). The ket $|ljR\tau IM\rangle$ describes the dependence on spin and angular coordinates of the particle and the orientation angle of the rotor, and is given by

$$|ljR\tau IM\rangle=\sum_{mM_R}\langle jmRM_R|IM\rangle|R\tau M_R\rangle|ljm\rangle. \tag{2}$$

This is the laboratory frame or *R*-representation as described in Eq. (2) of Ref. [11]. The total Hamiltonian of the proton-core system,

$$H=T+V(\mathbf{r},\omega)+V_{ls}(\mathbf{r},\omega)+H_R, \tag{3}$$

consists of the relative kinetic energy T, the nuclear plus Coulomb interaction $V(\mathbf{r},\omega)$, which depends on the position $\mathbf{r}$ of the proton and the orientation ω of the rotor in the space-fixed system, the deformed spin-orbit potential $V_{ls}(\mathbf{r},\omega)$, and the Hamiltonian H_R of the rotor. The detailed parametrization of the nuclear and Coulomb interactions are given in Appendix A, and the deformed spin-orbit term is discussed in Appendix B. To proceed, we first expand the potential $V(\mathbf{r},\omega)$ in the D functions, which are related to the spherical harmonics:

$$V(\mathbf{r},\omega)=\sum_{\lambda\mu}V_{\lambda\mu}(r)D^{\lambda}_{\mu 0}(\theta',\phi'), \tag{4}$$

$$V_{\lambda\mu}(r)=\frac{2\lambda+1}{4\pi}\int_{-1}^{1}d(\cos\,\theta')\times\int_0^{2\pi}d\phi' D^{\lambda *}_{\mu 0}(\theta',\phi')\;V(r,\theta',\phi'), \tag{5}$$

where θ',ϕ' refer to the angles of the particle with respect to the three-axis of the rotor. Because of reflection symmetry, λ and μ are restricted to even values (see Appendix A). Projecting with $|ljR\tau IM\rangle$ on the Schrödinger equation $H\Psi_{IM}$

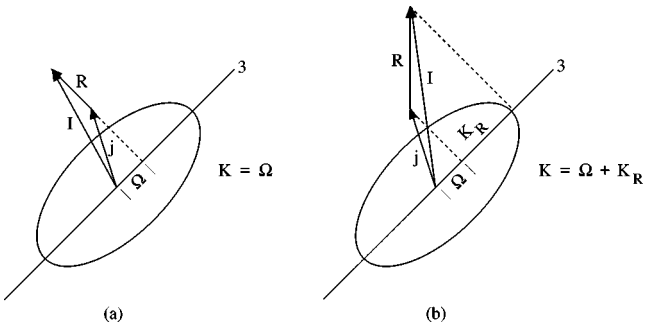

FIG. 1. (a) Relationship of the angular momentum vectors **j**, **R**, and **I** in the axially symmetric case. (b) Same as (a) except for the triaxial case. In both cases K is the projection of the total angular momentum **I** on the three-axis of the body-centered system.

$=E\Psi_{IM}$ we obtain a set of coupled equations in the radial wave functions

$$(h_{lj}+E_{R\tau}-E)\phi^I_{ljR\tau}(r) = -\sum_{l'j'R'\tau'}\sum_{\lambda>0,\mu}\langle ljR\tau IM|D^{\lambda}_{\mu 0}(\theta',\phi') \times|l'j'R'\tau' IM\rangle V_{\lambda\mu}(r)\phi^I_{l'j'R'\tau'}(r) - \sum_{l'j'R'\tau'}\langle ljR\tau IM|V_{ls}(\mathbf{r},\omega) \times|l'j'R'\tau' IM\rangle\phi^I_{l'j'R'\tau'}(r), \quad (6)$$

where

$$h_{lj}=\frac{\hbar^2}{2\mu_0}\left(-\frac{d^2}{dr^2}+\frac{l(l+1)}{r^2}\right)+V_0(r),$$

and $V_0(r)$ is the monopole part of the Coulomb plus nuclear potential. Here μ_0 is the proton reduced mass and $E_{R\tau}$ is the energy of the rotational state $|R\tau M_R\rangle$. In Appendix B we will extract the monopole part of the spin-orbit potential for inclusion in h_{lj}.

III. THE *K* REPRESENTATION

The matrix elements on the right-hand side of Eq. (6) are easiest to evaluate if we go over into the K representation of Ref. [11], which is expressed in the body-centered coordinates of the rotor. In this system the quantum number τ is identified with the projection K_R of R on the rotor's three-axis. For clarity, the quantum numbers m, M_R, and M in Eq. (2) all refer to angular momentum projections on the z axis of the space-fixed coordinate system due to the particle, rotor, and nucleus, respectively, while the corresponding projections on the three-axis in the body-fixed system are denoted by Ω, K_R, and K (see Fig. 1). As a consequence, the following relations hold:

$$M=M_R+m, \quad (7)$$

$$K=K_R+\Omega. \quad (8)$$

In the K representation we can write the transformed rotor wave function as **(**see Eqs. (4)–(7) of Ref. [15]**)**

$$\langle\omega|R\tau M_R\rangle=\langle\omega|RK_RM_R\rangle=\sqrt{\frac{2R+1}{8\pi^2}}D^R_{M_RK_R}(\omega), \quad (9)$$

which is a function of the orientation ω of the rotor in the laboratory frame. For an axially symmetric rotor, we would have $K_R=0$, resulting in $\Omega=K$ from Eq. (8). The particle wave function is

$$|ljm\rangle=\sum_{\Omega}D^j_{m\Omega}(\omega)|lj\Omega\rangle, \quad (10)$$

where the single-particle wave function $|lj\Omega\rangle$ is evaluated in the body-fixed frame of the rotor.

After inserting Eqs. (9) and (10) into Eq. (2), we may contract it using Eq. (1A-43) of [15], with the result

$$|ljRK_RIM\rangle=\sqrt{\frac{2R+1}{8\pi^2}}\sum_{K,\Omega}\langle j\Omega RK_R|IK\rangle D^I_{MK}(\omega)|lj\Omega\rangle. \quad (11)$$

Because the rotor possesses symmetry after rotating 180° around any of its three axes, it is convenient to have the projection K appear only as a positive number. Symmetry properties of the wave function require that the quantity $K_R=K-\Omega$ be an even integer $(0,\pm2,\pm4,\ldots)$ [16]. We then have

$$|ljRK_RIM\rangle=\sqrt{\frac{2R+1}{8\pi^2}}\sum_{K>0,\Omega}\langle j\Omega RK_R|IK\rangle[D^I_{MK}(\omega)|lj\Omega\rangle + (-1)^{I-j}D^I_{M-K}(\omega)|lj\bar{\Omega}\rangle], \quad (12)$$

where $\bar{\Omega}$ stands for $-\Omega$. Since we are only interested in the low-lying states of the rotor where $R=0,2,4,\ldots$, we rewrite Eq. (12) as

$$|ljRK_RIM\rangle=\sum_{K>0,\Omega}A^{IK}_{j\Omega,RK_R}|lj\Omega KIM\rangle, \quad (13)$$

where

$$A^{IK}_{j\Omega,RK_R}=\sqrt{\frac{2R+1}{2I+1}}\langle j\Omega RK_R|IK\rangle\sqrt{1+(-1)^R} \quad (14)$$

and

$$|lj\Omega KIM\rangle=\sqrt{\frac{2I+1}{16\pi^2}}[D^I_{MK}(\omega)|lj\Omega\rangle + (-1)^{I-j}D^I_{M-K}(\omega)|lj\bar{\Omega}\rangle]. \quad (15)$$

For an axially symmetric nucleus, K_R vanishes, making $\Omega=K$, and Eqs. (14) and (15) become identical to Eqs. (14) and (15) of Ref. [11].

Inserting Eq. (13) into Eq. (1) we can now express the total wave function in terms of the new basis (15):

$$\Psi_{IM}=\sum_{lj}\sum_{K>0}\sum_{\Omega}\frac{\phi^{IK}_{lj\Omega}(r)}{r}|lj\Omega KIM\rangle, \quad (16)$$

where the radial wave functions are

$$\phi^{IK}_{lj\Omega}(r) = \sum_{RK_R} A^{IK}_{j\Omega,RK_R}\phi^{I}_{ljRK_R}(r). \tag{17}$$

Note that the triaxial radial wave functions depend on the particle quantum number Ω in addition to lj.

It is easy to show that the amplitudes (14) form an orthonormal transformation between the K and the R representation, i.e.,

$$\sum_{K>0}\sum_{\Omega} A^{IK}_{j\Omega,RK_R}A^{IK}_{j\Omega,R'K_{R'}} = \delta_{R,R'}\delta_{K_R,K_{R'}},$$

$$\sum_{RK_R} A^{IK}_{j\Omega,RK_R}A^{IK'}_{j\Omega',RK_R} = \delta_{\Omega,\Omega'}\delta_{K,K'}. \tag{18}$$

Thus we can transform the results obtained in one representation into the other. After inverting Eq. (17) we obtain

$$\phi^{I}_{ljRK_R}(r) = \sum_{K>0}\sum_{\Omega} A^{IK}_{j\Omega,RK_R}\phi^{IK}_{lj\Omega}(r). \tag{19}$$

A. Coupled equations in the *K* representation

We continue with the evaluation of the matrix elements on the right-hand side (RHS) of Eq. (6). Inserting expression (13) for the spin-angular wave functions in the R representation we obtain

$$\langle ljRK_RIM|D^{\lambda}_{\mu 0}(\theta',\phi')|l'j'R'K_{R'}IM\rangle = \sum_{K>0}\sum_{K'>0}\sum_{\Omega,\Omega'} A^{IK}_{j\Omega,RK_R}\langle lj\Omega KIM|D^{\lambda}_{\mu 0}(\theta',\phi') \times|l'j'\Omega'K'IM\rangle A^{IK'}_{j'\Omega',R'K_{R'}}$$

and a similar expression for the matrix element of the spin-orbit potential. The advantage of using the K representation, Eq. (15), now becomes evident because each matrix element is the product of two parts. The first part involves integrating a product of orthogonal D functions over the orientation coordinates ω of the rotor, and yields the important result $\delta_{K,K'}$. The second part involves the single-particle wave functions in the body-fixed rest frame of the rotor:

$$\langle lj\Omega|D^{\lambda}_{\mu 0}(\theta',\phi')|l'j'\Omega'\rangle = (-1)^{\lambda}\left\langle j\tfrac{1}{2}\lambda 0|j'\tfrac{1}{2}\right\rangle\langle j'\Omega'\lambda\mu|j\Omega\rangle. \tag{20}$$

Thus

$$\langle ljRK_RIM|D^{\lambda}_{\mu 0}(\theta',\phi')|l'j'R'K_{R'}IM\rangle = \sum_{K'>0}\sum_{\Omega,\Omega'} A^{IK'}_{j\Omega,RK_R}\langle lj\Omega|D^{\lambda}_{\mu 0}(\theta',\phi')|l'j'\Omega'\rangle A^{IK'}_{j'\Omega',R'K_{R'}}. \tag{21}$$

For the spin-orbit potential we have a similar expression. We show how to evaluate the matrix elements of the spin-orbit interaction in Appendix B. Because the matrix elements are diagonal in K, Eq. (8) shows that the particle projections Ω,Ω' are restricted by $|\Omega-\Omega'|$=an even integer. We still have the previously determined restrictions λ even and $|K-\Omega|$=an even integer.

We now obtain the coupled equations in the K representation by multiplying Eq. (6) by $A^{IK}_{j\Omega,RK_R}$ and summing over RK_R, using Eqs. (17) and (18). The presence of the rotational energy E_{RK_R} requires the use of Eq. (19) for the radial wave function. Thus we obtain

$$(h_{lj}-E)\phi^{IK}_{lj\Omega}(r) + \sum_{K'>0}\sum_{\Omega'} W^{KK'}_{j\Omega\Omega'}\phi^{IK'}_{lj\Omega'}(r) = -\sum_{l'j'}\sum_{\Omega'}\left\{\sum_{\lambda>0,\mu}\langle lj\Omega|D^{\lambda}_{\mu 0}(\theta',\phi')|l'j'\Omega'\rangle V_{\lambda\mu}(r) + \langle lj\Omega|V_{ls}(\mathbf{r})|l'j'\Omega'\rangle\right\}\phi^{IK}_{l'j'\Omega'}(r), \tag{22}$$

where

$$W^{KK'}_{j\Omega\Omega'} = \sum_{RK_R} A^{IK}_{j\Omega,RK_R}E_{RK_R}A^{IK'}_{j\Omega',RK_R}. \tag{23}$$

To recover the axially symmetric case we set $\Omega=\Omega'=K$, and $\mu=0$ in Eqs. (22) and (23). This removes the sums over Ω', K_R, and μ.

B. Adiabatic limit

For a comparison with the results obtained in Ref. [11], we will solve the coupled equations (22) in the adiabatic limit, where the rotational energies E_{RK_R} of the core are set to zero. This sets equal to zero the second term on the left-hand side of Eq. (22). In this case we have

$$(h_{lj}-E)\phi^{IK}_{lj\Omega}(r) = -\sum_{l'j'\Omega'}\left\{\sum_{\lambda>0,\mu}\langle lj\Omega|D^{\lambda}_{\mu 0}(\theta',\phi') \times|l'j'\Omega'\rangle V_{\lambda\mu}(r) + \langle lj\Omega|V_{ls}(\mathbf{r}) \times|l'j'\Omega'\rangle\right\}\phi^{IK}_{l'j'\Omega'}(r). \tag{24}$$

The important thing to notice is that the coupled equations are then diagonal in K, but include Ω mixing. In other words, in the adiabatic limit, K is still a good quantum number, but, in addition to the $\Omega=K$ component, the interaction mixes into the wave function components with $\Omega=K\pm 2, K\pm 4$, etc., subject to the restriction $|\Omega|\leqslant j$. It should also be noted that the Clebsch-Gordan coefficient in Eq. (20) is nonzero only when $\Omega'+\mu=\Omega$.

The consequence of this Ω mixing is that the number of coupled equations will be substantially larger than is found in the axially symmetric case. As an example, consider the combinations of j and Ω needed to solve the equations for the $I=K=\frac{7}{2}^-$ ground state of the deformed proton emitter ^{141}Ho. The spherical states involved will be $j=\frac{7}{2}^-$, $\frac{9}{2}^-$, $\frac{11}{2}^-$, $\frac{13}{2}^-$, and $\frac{15}{2}^-$. In addition to $\Omega=K$, for each j there will be associated up to seven more values of Ω. Table I shows the permissible j,Ω combinations for the $I=K=\frac{7}{2}^-$ ground state of ^{141}Ho. The total number of wave function combinations is 30, which is to be contrasted with only 5 for the axially symmetric case.

TABLE I. Combinations of j and Ω for $I=K=\frac{7}{2}^-$ originating from $j=\frac{7}{2}^- \rightarrow \frac{15}{2}^-$. The bullet (•) denotes states occurring in the axially symmetric case.

j	Ω	Axially symmetric	j	Ω	Axially symmetric
$\frac{7}{2}^-$	$-\frac{5}{2}$		$\frac{13}{2}^-$	$-\frac{13}{2}$	
$\frac{7}{2}^-$	$-\frac{1}{2}$		$\frac{13}{2}^-$	$-\frac{9}{2}$	
$\frac{7}{2}^-$	$\frac{3}{2}$		$\frac{13}{2}^-$	$-\frac{5}{2}$	
$\frac{7}{2}^-$	$\frac{7}{2}$	•	$\frac{13}{2}^-$	$-\frac{1}{2}$	
$\frac{9}{2}^-$	$-\frac{9}{2}$		$\frac{13}{2}^-$	$\frac{3}{2}$	
$\frac{9}{2}^-$	$-\frac{5}{2}$		$\frac{13}{2}^-$	$\frac{7}{2}$	•
$\frac{9}{2}^-$	$-\frac{1}{2}$		$\frac{13}{2}^-$	$\frac{11}{2}$	
$\frac{9}{2}^-$	$\frac{3}{2}$		$\frac{15}{2}^-$	$-\frac{13}{2}$	
$\frac{9}{2}^-$	$\frac{7}{2}$	•	$\frac{15}{2}^-$	$-\frac{9}{2}$	
$\frac{11}{2}^-$	$-\frac{9}{2}$		$\frac{15}{2}^-$	$-\frac{5}{2}$	
$\frac{11}{2}^-$	$-\frac{5}{2}$		$\frac{15}{2}^-$	$-\frac{1}{2}$	
$\frac{11}{2}^-$	$-\frac{1}{2}$		$\frac{15}{2}^-$	$\frac{3}{2}$	
$\frac{11}{2}^-$	$\frac{3}{2}$		$\frac{15}{2}^-$	$\frac{7}{2}$	•
$\frac{11}{2}^-$	$\frac{7}{2}$	•	$\frac{15}{2}^-$	$\frac{11}{2}$	
$\frac{11}{2}^-$	$\frac{11}{2}$		$\frac{15}{2}^-$	$\frac{15}{2}$	

C. Decay rate calculation

We obtain the partial decay rate for proton emission from a state having angular momentum $I=K$ in the adiabatic limit via either the direct method (Dir) or the distorted wave (DW) Green's function method using Eq. (7) of Ref. [11]. While in the axially symmetric case the daughter states were labeled only by the quantum number R, in the triaxial case we need the second label τ or K_R as well:

$$\Gamma^I_{RK_R} = \sum_{lj} \Gamma^I_{ljRK_R} = \frac{\hbar^2 k_R}{\mu} \sum_{lj} |N^{I,Dir/DW}_{ljRK_R}|^2, \tag{25}$$

where

$$N^{I,Dir}_{ljRK_R} = \frac{\phi^I_{ljRK_R}(r)}{G_l(k_R r)} \quad \text{at } r = r_m,$$

$$N^{I,DW}_{ljRK_R} = -\frac{2\mu}{\hbar^2 k_R} \sum_{l'j'R'K_{R'}} \int_0^{r_{int}} dr F_l(k_R r) \langle ljRK_R IM | V(\mathbf{r},\omega) + V_{ls}(\mathbf{r},\omega) - \frac{Z_D e^2}{r} | l'j'R'K_{R'}IM\rangle \phi^I_{l'j'R'K_{R'}}(r). \tag{26}$$

Here k_R is the proton wave number for the decay to the daughter state with quantum numbers RK_R. Having obtained the radial wave function $\phi^{IK}_{lj\Omega}(r)$ for a given $K=I$ in the adiabatic limit, we can construct the associated radial wave functions in the R representation,

$$\phi^I_{ljRK_R}(r) = \sum_{\Omega} A^{IK}_{j\Omega,RK_R} \phi^{IK}_{lj\Omega}(r), \tag{27}$$

by means of Eq. (19). Inserting this wave function into Eq. (26), we obtain for the direct method

$$N^{I,Dir}_{ljRK_R} = \frac{1}{G_l(k_R r_m)} \sqrt{\frac{2(2R+1)}{2I+1}} \sum_{\Omega} \langle j\Omega RK_R | IK\rangle \phi^{IK}_{lj\Omega}(r_m). \tag{28}$$

Using this equation we can immediately see the effect of the triaxial shape on the decay rate: for decay to the ground state ($R=0$), the Clebsch-Gordan coefficient has the value $\delta_{j,I}\delta_{\Omega,K}$. Thus only the $\Omega=K$ component of the wave function will participate in this decay branch, effectively reducing its decay rate relative to that for the axially symmetric case since there are now other Ω components present in the triaxial wave function.

For the Green's function method, after performing the same operations that led to Eq. (21) to obtain the matrix elements of the interaction in Eq. (26), the second orthogonality relation in Eq. (18) allows the summations over R' and $K_{R'}$ to be performed. The final expression for the Green's function method is

$$N^{I,DW}_{ljRK_R} = -\frac{2\mu}{\hbar^2 k_R} \sum_{l'j'} \sum_{\Omega,\Omega'} A^{IK}_{j\Omega,RK_R} \int_0^{r_{int}} dr F_l(k_R r) \langle lj\Omega | V(\mathbf{r},\omega) + V_{ls}(\mathbf{r},\omega) - \frac{Z_D e^2}{r} | l'j'\Omega'\rangle \phi^{IK}_{l'j'\Omega'}(r). \tag{29}$$

This expression reduces to the analogous one for an axially symmetric nucleus when K is set equal to Ω and the sums over Ω and Ω' are removed.

IV. APPLICATIONS

In this section we use the formalism described above to calculate decay rates for the deformed proton emitter ^{141}Ho ($I=K=7/2^-$), in both the axially symmetric and triaxial cases. The calculations have been performed in the adiabatic limit, using the potential parameters found in Ref. [11]. The ground-state wave function was expanded in spherical components with $j=7/2^-$, $9/2^-$, $11/2^-$, $13/2^-$, and $15/2^-$. All multipole expansions were carried out up to $\lambda=14$. The results are compared with experimental values for the total decay width and the branching ratio for decay to the first excited 2^+ state in the daughter nucleus ^{140}Dy.

A. Axially symmetric case: The deformed proton emitter ^{141}Ho

To verify the formulation, we have computed the decay half-life and branching ratio to the 2^+ state in the daughter nucleus for the deformed proton emitter ^{141}Ho, using deformed spin-orbit matrix elements for the axially symmetric case ($\gamma=\mu=0$, $\Omega=\Omega'=K$) calculated from Eq. (B17), which, again for $\lambda>0$, now reads

$$\langle ljK | V_{ls}(r,\theta) | l'j'K\rangle = 2V_{so} \sum_{\lambda>0} \frac{\langle j'K\lambda 0 | jK\rangle}{\sqrt{2j+1}} \times \langle lj \| [\nabla f_{\lambda\mu}(r) D^{\lambda}_{\mu 0}(\hat{\mathbf{r}})] \cdot (-i\nabla \times \hat{\sigma}) \| l'j'\rangle, \tag{30}$$

TABLE II. Comparison of calculated and experimental values for ^{141}Ho$(7/2^-)$ total decay rate and 2^+ branching ratio. Input values are $E_x(2^+)$ in ^{140}Dy=202 keV, $\beta_2=0.244$, and $\beta_4=-0.046$. Calculations were done in the adiabatic limit, with no static triaxiality, and uncertainties coming from the measured proton energy of 1169(8) keV [17] and the decay half-life of 4.2(4) ms [17] have been taken into account. The experimental spectroscopic factor $S_{\rm expt}$ is defined as $\Gamma_{\rm expt}/\Gamma_{\rm calc}$. The calculated spectroscopic factor $S_{\rm calc}=u^2$ is obtained from a BCS calculation (see text).

$\Gamma_{\rm calc}(10^{-19}$ MeV)	$\Gamma_{\rm expt}(10^{-19}$ MeV)	$S_{\rm calc}$	$S_{\rm expt}$	$BR(2^+)_{\rm calc}$	$BR(2^+)_{\rm expt}$
$1.51^{+0.34}_{-0.28}$	1.09(10)[a]	0.6	$0.72^{+0.17}_{-0.15}$	0.0071(5)	0.0070(15)[b]

[a]Reference [17].
[b]Reference [18].

where the reduced matrix element is that calculated in Eq. (B16). The results of the calculations are shown in Table II, and are identical with those obtained using the axially symmetric deformed spin-orbit term of Ref. [11]. It should be noted that the numbers obtained here and in Ref. [11] differ slightly, since the 2^+ excitation energy of 202 keV in the daughter nuclide ^{140}Dy used here has only recently been measured [19,20], and was not known when the calculations in Ref. [11] were carried out. In that work an excitation energy of 166 keV was used.

B. Triaxial case: The deformed proton emitter ^{141}Ho

As previously mentioned, particle-rotor calculations of the energy levels in the rotational band lying above the $I=7/2^-$ ground state of the deformed proton emitter ^{141}Ho were reported in Ref. [12]. These calculations suggest that better agreement with experiment would be obtained with the introduction of a small amount of static triaxial deformation. In order to assess the effect on the proton decay rates of adding such a deformation, we have used the formalism developed in the present work to compute, in the adiabatic limit, the decay rate and 2^+ branching ratio for this proton emitting nuclide, as a function of the angle of triaxiality γ. The calculations were performed with $\beta_2=0.244$, $\beta_4=-0.046$.

Figure 2 shows the product of calculated total decay width $\Gamma_{\rm calc}$ and spectroscopic factor $S_{\rm calc}=u^2=0.6$ for the ^{141}Ho ground state, plotted as a function of the triaxial angle γ. The spectroscopic factor was obtained from a BCS calculation, using a proton pairing gap Δ_p of 0.9 MeV. The shaded area represents the experimental measurement, and the error bar attached to the calculated curve represents the uncertainty in the calculated width due to the uncertainty in the proton energy. It is seen that calculation and experiment agree well for small values of γ.

Figure 3 shows the calculated 2^+ branching ratio, plotted as a function of γ, along with the experimental value, 0.0070(15) [18]. The small error bar on the calculated curve is due to the uncertainty in the proton energy. The agreement between calculation and experiment is excellent for small values of γ, and this suggests that a static triaxial deformation, if present, is limited to an angle of $\leqslant 5°$.

Plotted in Fig. 4 are the amplitudes for the allowed Ω values of $+7/2^-$, $+3/2^-$, $-1/2^-$, and $-5/2^-$ for the $j=7/2$ spherical component of the ^{141}Ho ground-state wave function. As expected, for $\gamma=0$, only the $\Omega=+7/2^-$ component is present, but with increasing γ, other Ω components differing by $\pm 2, \pm 4, \ldots$ begin to mix into the wave function. The decay proceeds primarily to the daughter ground state, and only the $\Omega=+7/2^-$ component participates in this branch. Thus the decrease in the total decay width with increasing γ seen in Fig. 2 tracks with the decrease in the $\Omega=+7/2^-$ wave function component, which itself follows from the increasing appearance of other Ω values in the wave function.

V. CONCLUSIONS

In this work we have developed a formalism to include the effect of static triaxial deformation on calculations of the decay rate for a deformed nucleus. The main complications over the axially symmetric case are the additional dependence of the interaction potential on the proton azimuthal angle ϕ, and a consequent increase in the complexity of the deformed spin-orbit potential. The extra dimension causes additional Ω components to be introduced into the wave function. The matrix elements of the spin-orbit interaction

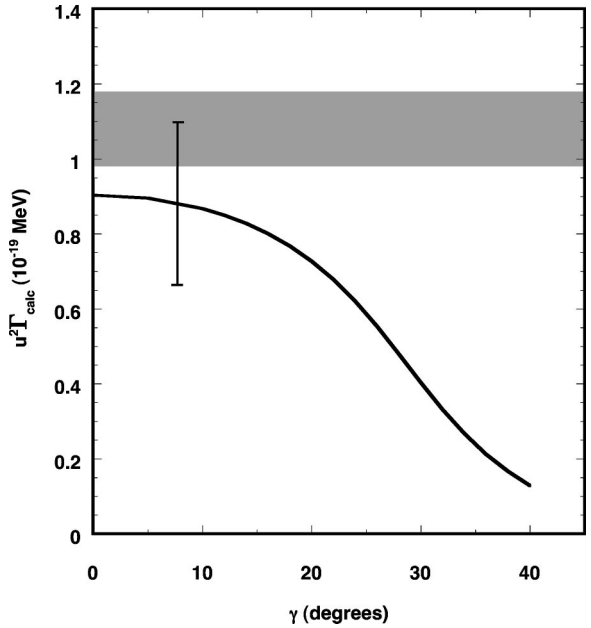

FIG. 2. Calculated total decay width, in units of 10^{-19} MeV, for ^{141g}Ho, plotted as a function of the triaxial angle γ. The shaded area represents the experimental measurement, and the error bar attached to the calculated curve represents the uncertainty in the calculated width due to the uncertainty in the proton energy.

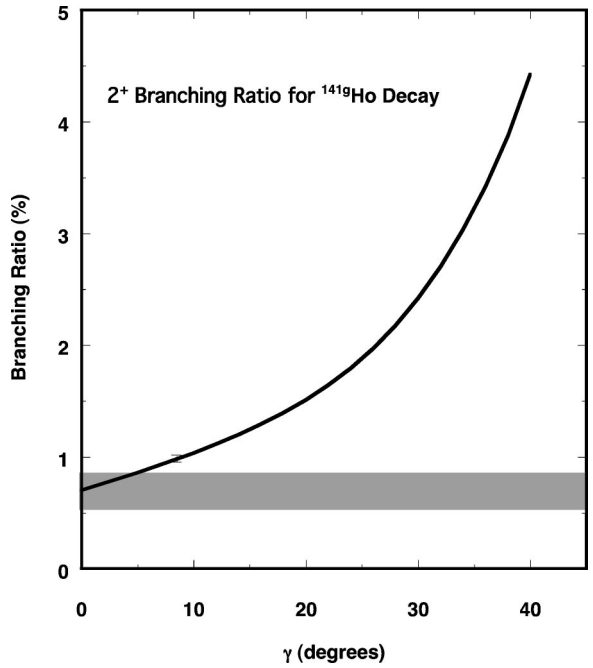

FIG. 3. Calculated branching ratio in percent for the decay of ^{141g}Ho to the 2^+ state of ^{140}Dy at an excitation energy of 202 keV, plotted as a function of the triaxial angle γ. The shaded area represents the experimental measurement, and the error bar attached to the calculated curve represents the uncertainty in the calculated branching ratio due to the uncertainty in the proton energy.

have been calculated using a tensor algebra approach, as described in Appendix B.

We have applied the above mentioned methodology to calculations of the decay rate of the deformed proton emitter

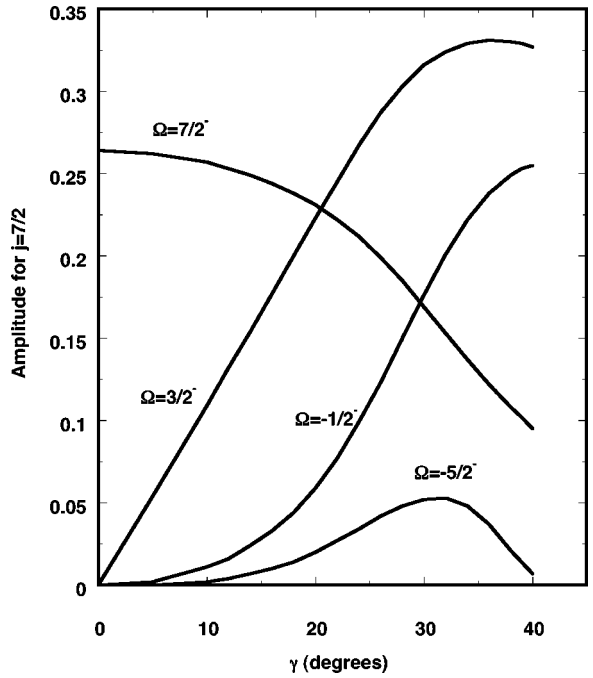

FIG. 4. Amplitudes for various Ω values of the $j=7/2^-$ component of the ^{141g}Ho wave function, plotted as a function of the triaxial angle γ.

^{141g}Ho, which has spin-parity $7/2^-$. In Ref. [11] it was shown that the nonadiabatic coupled-channels approach does not yield results for ^{141g}Ho decay which agree with experiment, either for the absolute decay rate or the branching ratio for decay to the first 2^+ of the daughter nucleus ^{140}Dy. This is because of the presence of Coriolis mixing, which is particularly strong for high spin states. Empirically it is known that it is necessary to quench the Coriolis mixing in order to obtain good agreement with data [21,22]. It was found in Ref. [11] that good agreement with experiment was obtained in the adiabatic limit, where the energies of the rotational states of the daughter nucleus are set to zero. For this reason we have performed the triaxial calculations in the adiabatic limit.

After first checking the results of the calculation against an axially symmetric code, triaxiality was introduced, ranging up to a γ angle of 40°. While the sensitivity of the resulting total decay rate to triaxial angle γ was not high, the calculation of the branching ratio for decay to the first 2^+ state of the daughter showed a strong dependence on γ, essentially ruling out angles greater than 5°. We believe that the branching ratio calculation is quite reliable, since factors such as absolute spectroscopic factors tend to cancel.

In conclusion, we do not believe that a static triaxial deformation plays an important role in helping to explain the decay rate of the deformed proton emitter ^{141g}Ho. Triaxiality may still exert an influence on the nuclear structure of this nuclide, but most likely at higher spins and excitation energies.

ACKNOWLEDGMENTS

We wish to acknowledge valuable discussions with K. Hagino. This work was supported by the U.S. Department of Energy, Nuclear Physics Division, under Contract No. W-31-109-ENG-38.

APPENDIX A: PARAMETRIZATION OF THE INTERACTION POTENTIAL

For triaxial nuclei, the degree of triaxiality is denoted by the angle γ, which is one of the Hill-Wheeler [23] coordinates. We parametrize the nuclear interaction between the valence proton and the deformed core nucleus in terms of the Fermi function $f(x)=[1+\exp(x)]^{-1}$ as

$$V_N(r,\theta,\phi) = V_N^{(0)} f\left(\frac{r - R(\theta,\phi)}{a(\theta)}\right), \tag{A1}$$

where $V_N^{(0)}$ is the depth of the nuclear potential, $a(\theta)$ is an angle-dependent diffuseness as in Eq. (A6) of Ref. [11], and

$$R(\theta,\phi) = R_N\left\{1 + \sum_{\mu=-2,even}^{2} a_{2\mu} Y_{2\mu}(\theta,\phi) + \sum_{\mu=-4,even}^{4} a_{4\mu} Y_{4\mu}(\theta,\phi)\right\}. \tag{A2}$$

Here (θ,ϕ) are the angles between $\mathbf{r}$ and the three-axis of the core, and

$$a_{20} = \beta_2 \cos\gamma, \quad a_{22} = a_{2-2} = \frac{\beta_2 \sin\gamma}{\sqrt{2}},$$

$$a_{40} = \frac{1}{6}\beta_4(5\cos^2\gamma + 1),$$

$$a_{42} = a_{4-2} = -\frac{1}{12}\beta_4\sqrt{30}\sin 2\gamma, \tag{A3}$$

$$a_{44} = a_{4-4} = \frac{1}{12}\beta_4\sqrt{70}\sin^2\gamma.$$

The radius is calculated as

$$R_N = r_0\left(\frac{A_D}{C(\beta_2,\beta_4,\gamma)}\right)^{1/3}, \tag{A4}$$

where

$$C(\beta_2,\beta_4) = \int \frac{d\Omega}{4\pi}\left(1 + \sum_{\mu=-2,even}^{2} a_{2\mu}Y_{2\mu}(\theta,\phi) + \sum_{\mu=-4,even}^{4} a_{4\mu}Y_{4\mu}(\theta,\phi)\right)^3 \tag{A5}$$

is the volume preserving factor and A_D is the mass number of the core. Equations (A2) and (A5) reduce to Eqs. (A1) and (A2) of Ref. [11] for the axially symmetric case ($\mu=\gamma=0$). Values of $r_0=1.25$ fm and $a=0.65$ fm are used in our calculations.

We parametrize the charge density of the core in a similar way, using the slightly different radial parameters of $r_0=1.22$ fm and $a_C=0.56$ fm, as was done in Ref. [11].

APPENDIX B: DEFORMED SPIN-ORBIT POTENTIAL

For the solution of the coupled equations, Eq. (24), matrix elements of the spin-orbit potential $\langle lj\Omega|V_{ls}(r,\theta,\phi)|l'j'\Omega'\rangle$ are needed. As in Ref. [11] we use a deformed spin-orbit potential, but with the addition of ϕ-dependent terms not found there. We follow the tensor algebra approach of Hagino [24], who has calculated matrix elements of the spin-orbit interaction in the context of particle-vibration coupling for spherical nuclei.

The starting point is to express the deformed spin-orbit interaction in the Thomas form [11] with the deformed Fermi function of Eq. (A1):

$$V_{ls}(r,\theta,\phi) = 4V_{so}\left(\left[\nabla f\left(\frac{r-R(\theta,\phi)}{a(\theta)}\right)\right]\times\mathbf{p}\cdot\mathbf{s}\right). \tag{B1}$$

We now make a multipole expansion of the Fermi function

$$f(r,\theta,\phi) = \sum_{\lambda\mu} f_{\lambda\mu}(r)D^{\lambda}_{\mu 0}(\hat{\mathbf{r}}), \tag{B2}$$

$$f_{\lambda\mu}(r) = \frac{2\lambda+1}{4\pi}\int D^{\lambda *}_{\mu 0}(\hat{\mathbf{r}})f(r,\theta,\phi)d(\cos\theta)d\phi,$$

$$\frac{df_{\lambda\mu}(r)}{dr} = \frac{2\lambda+1}{4\pi}\int D^{\lambda *}_{\mu 0}(\hat{\mathbf{r}})\frac{df(r,\theta,\phi)}{dr}d(\cos\theta)d\phi. \tag{B3}$$

So

$$\begin{aligned} V_{ls}(r,\theta,\phi) &= 4V_{so}\Big(\sum_{\lambda\mu}[\nabla f_{\lambda\mu}(r)D^{\lambda}_{\mu 0}(\hat{\mathbf{r}})]\times\mathbf{p}\cdot\mathbf{s}\Big) \\ &= 4V_{so}\Bigg(\frac{1}{r}\frac{df_{00}(r)}{dr}D^{0}_{00}(\hat{\mathbf{r}})(\mathbf{r}\times\mathbf{p})\cdot\mathbf{s} \\ &\quad + \sum_{\lambda>0,\mu}[\nabla f_{\lambda\mu}(r)D^{\lambda}_{\mu 0}(\hat{\mathbf{r}})]\times\mathbf{p}\cdot\mathbf{s}\Bigg) \\ &= 4V_{so}\Bigg(\frac{1}{r}\frac{df_{00}(r)}{dr}\mathbf{l}\cdot\mathbf{s} \\ &\quad + \frac{1}{2}\sum_{\lambda>0,\mu}[\nabla f_{\lambda\mu}(r)D^{\lambda}_{\mu 0}(\hat{\mathbf{r}})]\cdot(-i\nabla\times\hat{\sigma})\Bigg). \end{aligned} \tag{B4}$$

The first term on the RHS of Eq. (B4) is the monopole part of the spin-orbit potential,

$$V^0_{ls}(r) = 4V_{so}\frac{1}{r}\frac{df_{00}(r)}{dr}\mathbf{l}\cdot\mathbf{s}, \tag{B5}$$

which can easily be incorporated into the monopole part of the Hamiltonian. The second term,

$$\delta V_{ls}(r,\theta,\phi) = V_{ls}(r,\theta,\phi) - V^0_{ls}(r), \tag{B6}$$

can be decomposed into a sum of angular momentum tensors involving the spherical harmonics $Y_{\lambda\mu}(\hat{\mathbf{r}})$, using the gradient formula, Eq. (5.9.17) of Ref. [25]:

$$\begin{aligned} &[\nabla f_{\lambda\mu}(r)D^{\lambda}_{\mu 0}(\hat{\mathbf{r}})]\cdot(-i\nabla\times\hat{\sigma}) \\ &= -\frac{\sqrt{4\pi(\lambda+1)}}{2\lambda+1}\left(\frac{df_{\lambda\mu}(r)}{dr} - \frac{\lambda}{r}f_{\lambda\mu}(r)\right) \\ &\quad\times[Y_{\lambda+1}(-i\nabla\times\hat{\sigma})]^{\lambda\mu} \\ &\quad + \frac{\sqrt{4\pi\lambda}}{2\lambda+1}\left(\frac{df_{\lambda\mu}(r)}{dr} + \frac{\lambda+1}{r}f_{\lambda\mu}(r)\right) \\ &\quad\times[Y_{\lambda-1}(-i\nabla\times\hat{\sigma})]^{\lambda\mu} \\ &= \frac{\sqrt{4\pi}}{2\lambda+1}\{\sqrt{\lambda}Q_{\lambda\mu}(r)T^{\lambda\mu}_{-} - \sqrt{\lambda+1}P_{\lambda\mu}(r)T^{\lambda\mu}_{+}\}, \end{aligned} \tag{B7}$$

where

$$T^{\lambda\mu}_{\pm} = [Y_{\lambda\pm1}(-i\nabla\times\hat{\sigma})]^{\lambda\mu}, \tag{B8}$$

$$P_{\lambda\mu}(r) = \frac{df_{\lambda\mu}(r)}{dr} - \frac{\lambda}{r}f_{\lambda\mu}(r),$$

and

$$Q_{\lambda\mu}(r) = \frac{df_{\lambda\mu}(r)}{dr} + \frac{\lambda+1}{r}f_{\lambda\mu}(r).$$

To solve the coupled radial equations we need to obtain the matrix elements of the operator $\Sigma_{\lambda>0,\mu}[\nabla f_{\lambda\mu}(r)D^{\lambda}_{\mu 0}(\hat{\mathbf{r}})]\cdot(-i\nabla\times\hat{\sigma})$, or specifically, the matrix elements of $\Sigma_{\lambda>0,\mu}\,T^{\lambda\mu}_{\pm}$ between spin-angular momentum states. This is done by using the Wigner-Eckart theorem,

$$\langle lj\Omega|T_{\pm}^{\lambda\mu}|l'j'\Omega'\rangle = \langle j'\Omega'\lambda\mu|j\Omega\rangle\frac{\langle lj\|T_{\pm}^{\lambda}\|l'j'\rangle}{\sqrt{2j+1}}, \quad \text{(B9)}$$

along with reduced matrix elements given in Eqs. (58) and (59) of Ref. [26] and Eq. (A2.14) of Ref. [27]. Equation (B9) is the point of departure between axially symmetric and triaxial calculations of the spin-orbit matrix elements, since the reduced matrix elements are independent of the projection quantum numbers Ω', Ω, and μ. For axial symmetry we will set $\Omega=\Omega'=K$ and $\gamma=\mu=0$.

Putting $L_{\pm}=\lambda\pm1$ we have

$$\begin{aligned}\langle lj\|T_{\pm}^{\lambda}\|l'j'\rangle &= \langle lj\|[Y_{L_{\pm}}(-i\boldsymbol{\nabla}\times\hat{\sigma})]^{\lambda}\|l'j'\rangle \\ &= \sum_{l_\alpha j_\alpha}(-1)^{\lambda+j+j'+1}\times\sqrt{36(2\lambda+1)(2j'+1)(2j_\alpha+1)} \\ &\times\begin{Bmatrix} L_{\pm} & 1 & \lambda \\ j' & j & j_\alpha\end{Bmatrix}\begin{Bmatrix} l_\alpha & l' & 1 \\ \frac{1}{2} & \frac{1}{2} & 1 \\ j_\alpha & j' & 1\end{Bmatrix}\langle lj\|Y_{L_{\pm}}\|l_\alpha j_\alpha\rangle \\ &\times\langle Y_{l_\alpha}\|\boldsymbol{\nabla}\|Y_{l'}\rangle, \end{aligned} \quad \text{(B10)}$$

where

$$\langle lj\|Y_{L_{\pm}}\|l_\alpha j_\alpha\rangle = (-1)^{1/2+j}\sqrt{\frac{(2j+1)(2L_{\pm}+1)(2j_\alpha+1)}{4\pi}}\times\begin{pmatrix} j & L_{\pm} & j_\alpha \\ \frac{1}{2} & 0 & -\frac{1}{2}\end{pmatrix} \quad \text{(B11)}$$

and

$$\langle Y_{l_\alpha}\|\boldsymbol{\nabla}\|Y_{l'}\rangle = \sqrt{2l'+1}\langle l'010|l_\alpha0\rangle\left[\frac{d}{dr}+\frac{1}{r}+\frac{1}{2r}\{l'(l'+1)-l_\alpha(l_\alpha+1)\}\right]. \quad \text{(B12)}$$

From the properties of the Clebsch-Gordan coefficient in Eq. (B12) it can be seen that l_α can take on only two values $l'\pm1$, indicating that the parity of $l_\alpha j_\alpha$ is opposite to that of $l'j'$ and lj. The permissible values of j_α in the summation in Eq. (B10) are $j_\alpha=l_\alpha\pm1/2$, and may be further restricted by the triangle relations for the $6j$ symbol, namely, $\Delta(L_{\pm}jj_\alpha)$ and $\Delta(j'1j_\alpha)$. Additionally, for the calculation of the matrix elements, the d/dr term in Eq. (B12) needs to be modified, since the coupled equations are in the wave function $\phi_l(r)$, while the Hamiltonian (3) acts on the wave function (1), which contains $\phi_l(r)/r$. Since

$$r\frac{d}{dr}\left(\frac{\phi_l(r)}{r}\right) = \frac{d\phi_l(r)}{dr}-\frac{\phi_l(r)}{r}, \quad \text{(B13)}$$

we see that the operator d/dr must be replaced by $(d/dr-1/r)$ in the coupled equations for $\phi_l(r)$. This replacement has been performed below.

Finally, after noting that λ is always even in this application, we have

$$\frac{\sqrt{4\pi}}{2\lambda+1}\langle lj\|T_{\pm}^{\lambda}\|l'j'\rangle = C^{\lambda}(j'jL_{\pm})\sum_{l_\alpha j_\alpha}A^{\lambda}(j_\alpha j'jL_{\pm})\times\left[\frac{d}{dr}+\frac{1}{2r}\{l'(l'+1)-l_\alpha(l_\alpha+1)\}\right], \quad \text{(B14)}$$

where

$$C^{\lambda}(j'jL_{\pm}) = (-1)^{j'+1/2}\times\sqrt{\frac{36(2j'+1)(2L_{\pm}+1)(2j+1)(2l'+1)}{(2\lambda+1)}}, \quad \text{(B15)}$$

and

$$A^{\lambda}(j_\alpha j'jL_{\pm}) = (2j_\alpha+1)\begin{Bmatrix} L_{\pm} & 1 & \lambda \\ j' & j & j_\alpha\end{Bmatrix}\begin{Bmatrix} l_\alpha & l' & 1 \\ \frac{1}{2} & \frac{1}{2} & 1 \\ j_\alpha & j' & 1\end{Bmatrix}\times\begin{pmatrix} j & L_{\pm} & j_\alpha \\ \frac{1}{2} & 0 & -\frac{1}{2}\end{pmatrix}\langle l'010|l_\alpha0\rangle.$$

After some rearrangement, we can write the reduced matrix element of the operator $[\boldsymbol{\nabla}f_{\lambda\mu}(r)D^{\lambda}_{\mu0}(\hat{\mathbf{r}})]\cdot(-i\boldsymbol{\nabla}\times\hat{\sigma})$ as

$$\begin{aligned}&\langle lj\|[\boldsymbol{\nabla}f_{\lambda\mu}(r)D^{\lambda}_{\mu0}(\hat{\mathbf{r}})]\cdot(-i\boldsymbol{\nabla}\times\hat{\sigma})\|l'j'\rangle \\ &= \left\{\sqrt{\lambda}Q_{\lambda\mu}(r)C^{\lambda}(j'jL_{-})\sum_{l_\alpha j_\alpha}A^{\lambda}(j_\alpha j'jL_{-})\right. \\ &\left.-\sqrt{\lambda+1}P_{\lambda\mu}(r)C^{\lambda}(j'jL_{+})\sum_{l_\alpha j_\alpha}A^{\lambda}(j_\alpha j'jL_{+})\right\}\frac{d}{dr} \\ &+\frac{1}{2r}\left\{\sqrt{\lambda}Q_{\lambda\mu}(r)C^{\lambda}(j'jL_{-})\sum_{l_\alpha j_\alpha}A^{\lambda}(j_\alpha j'jL_{-})[l'(l'+1)\right. \\ &\left.-l_\alpha(l_\alpha+1)]\right\}-\frac{1}{2r}\{\sqrt{\lambda+1}P_{\lambda\mu}(r)C^{\lambda}(j'jL_{+}) \\ &\times\sum_{l_\alpha j_\alpha}A^{\lambda}(j_\alpha j'jL_{+})[l'(l'+1)-l_\alpha(l_\alpha+1)]\}. \end{aligned} \quad \text{(B16)}$$

Recall that our original goal is to compute the spin-angular coupling matrix elements of the deformed spin-orbit interaction. For $\lambda>0$ we have, from Eqs. (B4) and (B9),

$$\langle lj\Omega|\delta V_{ls}(r,\theta,\phi)|l'j'\Omega'\rangle = 2V_{so}\sum_{\lambda>0,\mu}\frac{\langle j'\Omega'\lambda\mu|j\Omega\rangle}{\sqrt{2j+1}}\times\langle lj\|[\boldsymbol{\nabla}f_{\lambda\mu}(r)D^{\lambda}_{\mu0}(\hat{\mathbf{r}})]\cdot(-i\boldsymbol{\nabla}\times\hat{\sigma})l'j'\rangle. \quad \text{(B17)}$$

[1] P. J. Woods and C. N. Davids, Annu. Rev. Nucl. Part. Sci. **47**, 541 (1997).
[2] P. Möller *et al.*, At. Data Nucl. Data Tables **59**, 185 (1995).
[3] V. P. Bugrov and S. G. Kadmensky, Sov. J. Nucl. Phys. **49**, 967 (1989).
[4] S. G. Kadmensky and V. P. Bugrov, Phys. At. Nucl. **59**, 399 (1996).
[5] L. S. Ferreira, E. Maglione, and R. J. Liotta, Phys. Rev. Lett. **78**, 1640 (1997).
[6] E. Maglione, L. S. Ferreira, and R. J. Liotta, Phys. Rev. Lett. **81**, 538 (1998).
[7] E. Maglione, L. S. Ferreira, and R. J. Liotta, Phys. Rev. C **59**, R589 (1999).
[8] A. A. Sonzogni *et al.*, Phys. Rev. Lett. **83**, 1116 (1999).
[9] A. T. Kruppa *et al.*, Phys. Rev. Lett. **84**, 4549 (2000).
[10] B. Barmore *et al.*, Phys. Rev. C **62**, 054315 (2000).
[11] H. Esbensen and C. N. Davids, Phys. Rev. C **63**, 014315 (2001).
[12] D. Seweryniak *et al.*, Phys. Rev. Lett. **86**, 1458 (2001).
[13] C. N. Davids and H. Esbensen, *Proceedings of the Second International Symposium on Proton-Emitting Nuclei*, edited by E. Maglione and F. Soramel, AIP Conf. Proc. No. 681 (AIP, Melville, NY, 2003), p. 41.
[14] A. T. Kruppa and W. Nazarewicz, *Proceedings of the Second International Symposium on Proton-Emitting Nuclei*, Ref. [13], p. 61.
[15] A. Bohr and B. R. Mottelson, *Nuclear Structure* (Benjamin, Reading, MA, 1975), Vol. II.
[16] A. Bohr, Mat. Fys. Medd. K. Dan. Vidensk. Selsk. **26**, 14 (1952).
[17] C. N. Davids *et al.*, Phys. Rev. Lett. **80**, 1849 (1998).
[18] K. Rykaczewski *et al.* in *Mapping the Triangle*, edited by Ani Aprahamian, Jolie A. Cizewski, Stuart Pittel, and N. Victor Zamfir, AIP Conf. Proc. No. 638 (AIP, Melville, NY, 2002).
[19] D. Cullen *et al.*, Phys. Lett. B **529**, 42 (2002).
[20] W. Królas *et al.*, Phys. Rev. C **65**, 031303 (2002).
[21] A. Henriquez, T. Engeland, and J. Rekstad, Phys. Rev. C **27**, 1302 (1983).
[22] G. Fiorin, E. Maglione, and L. S. Ferreira, Phys. Rev. C **67**, 054302 (2003).
[23] D. L. Hill and J. A. Wheeler, Phys. Rev. **89**, 1102 (1953).
[24] K. Hagino, Phys. Rev. C **64**, 041304(R) (2001).
[25] A. R. Edmonds, *Angular Momentum in Quantum Mechanics* (Princeton University Press, Princeton, 1974).
[26] P.-G. Reinhard and Y. K. Gambhir, Ann. Phys. (Leipzig) **1**, 598 (1992).
[27] R. D. Lawson, *Theory of the Nuclear Shell Model* (Oxford University Press, Oxford, 1980).